

p-Type Co Interstitial Defects in Thermoelectric Skutterudite CoSb_3 Due to the Breakage of Sb_4 -Rings

Guodong Li,^{†,‡} Saurabh Bajaj,[§] Umut Aydemir,[‡] Shiqiang Hao,[‡] Hai Xiao,[†] William A. Goddard, III,^{*,†} Pengcheng Zhai,[†] Qingjie Zhang,^{*,†} and G. Jeffrey Snyder^{*,‡}

[†]State Key Laboratory of Advanced Technology for Materials Synthesis and Processing, Wuhan University of Technology, Wuhan, Hubei 430070, China

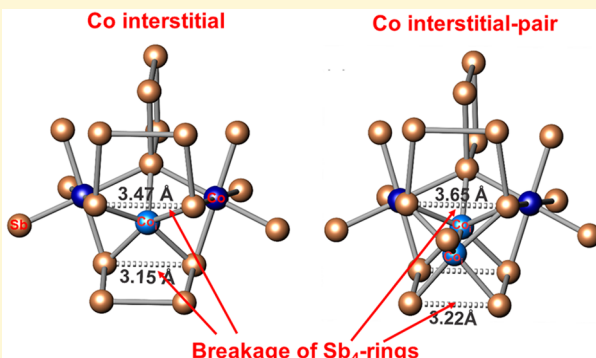
[‡]Department of Materials Science and Engineering, Northwestern University, Evanston, Illinois 60208, United States

[§]Environmental Energy & Technologies Division, Lawrence Berkeley National Laboratory, Berkeley, California 94720, United States

⁺Materials and Process Simulation Center, California Institute of Technology, Pasadena, California 91125, United States

Supporting Information

ABSTRACT: Skutterudite CoSb_3 based thermoelectric devices have high potential for engineering applications because both n- and p-type doped CoSb_3 demonstrate excellent thermoelectric performance. A crucial point concerning the application of CoSb_3 is to understand and control its defect chemistry. To reveal the native conductivity behavior of nonstoichiometric CoSb_3 , we investigated the intrinsic point defects in CoSb_3 using density functional theory. We found CoSb_3 is p-type in either Co or Sb rich regions of phase stability. Interstitial Co (Co_i) and interstitial Co-pair (Co_{i-p}) are the dominant point defects in the Co rich region. However, Co_{i-p} will be difficult to form because the formation temperature of Co_{i-p} is much lower than the synthesis temperature of CoSb_3 . The unexpected acceptor nature of the Co_i or Co_{i-p} defects is explained by the breakage of multiple Sb_4 -rings. Co vacancy (Co_v) is found to be the p-type defect in the Sb rich region. Furthermore, the solubility of excess Co in CoSb_3 is expected to be larger than that of Sb because of the lower formation energy and higher carrier concentration of Co_i compared with those of Co_v .



1. INTRODUCTION

Thermoelectric (TE) devices, consisting of coupled n- and p-type legs, can directly convert heat into electricity and are being considered for recovery of automobile exhaust heat.¹ Skutterudite CoSb_3 TE material, which can be obtained with both n- and p-type carriers, attracts worldwide attention because both heavily doped n- and p-type CoSb_3 display excellent TE properties.^{2,3} This makes careful analysis of the crystal structure and the transport properties of CoSb_3 necessary for its commercial applications.

Nominally pure CoSb_3 has been reported with either p- or n-type behavior with a small extrinsic carrier concentration less than $5 \times 10^{18} \text{ cm}^{-3}$.⁴⁻¹⁶ Generally, CoSb_3 is reported with p-type conductivity for both Co rich or Sb rich compositions.^{4-6,10-16} For example, p-type CoSb_3 in Sb rich composition has been prepared using a Bridgman gradient freeze technique, a solid state reaction method, or spark plasma sintering (SPS).^{4-6,10,12} p-type CoSb_3 in Co rich samples have been synthesized using a mechanical alloying (MA) method, a solid state reaction, and a melting method.^{11,15,16} Sometimes, n-type CoSb_3 can be obtained at room temperature which changes to p-type behavior with increasing temperature indicating that extrinsic carrier concentrations are small and

the mobility ratio of p-type to n-type is large.^{10,11,17,18} The inconsistency of these experimental results could be due to different raw materials used.

Nevertheless, understanding and controlling the intrinsic defects are an essential first step for the preparation and carrier optimization of CoSb_3 with excellent TE properties. Park et al. found that Co interstitial (Co_i) and Co vacancy (Co_v) are the p-type impurities in Co rich and Sb rich regions, respectively, and Co_{i-p} leads to the n-type defect in the Co rich region.¹⁹ However, it is expected that the charge state of Co atom in CoSb_3 is +3,³ and so Co_i would be expected to be an n-type donor defect, which is unexplained with Park's study.

In this paper, we used density functional theory (DFT) with the Perdew–Burke–Ernzerhof (PBE) functional to reveal the nature of the intrinsic defect in CoSb_3 . We found that the breakage of Sb_4 -rings induced by Co_i and Co_{i-p} defects is the source of p-type CoSb_3 in the Co rich region. In the Co_i defect, Co_i breaks two Sb–Sb bonds leading Co_i as a p-type defect with -1 charge state (see Figure 4). In the Co_{i-p} defect,

Received: January 10, 2016

Revised: February 18, 2016

Published: March 22, 2016

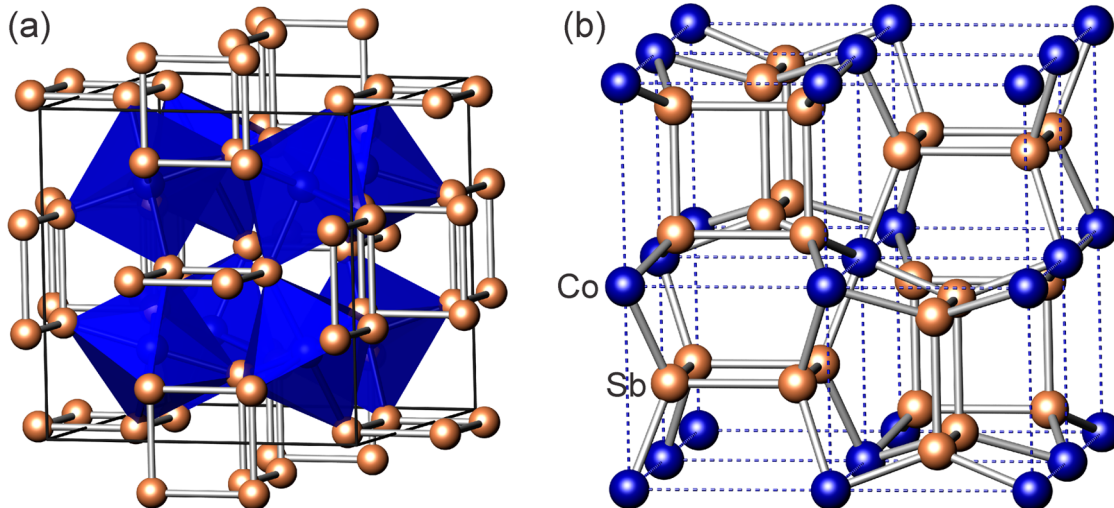


Figure 1. (a) The crystal structure of CoSb₃ with CoSb₆ octahedra (shown in blue) and Sb₄ rings. The Co and Sb atoms are represented with blue and brown colors, respectively. (b) In the unit cell, 6 out of 8 cubes formed by Co atoms encapsulate Sb₄ rings.

breaks three Sb–Sb bonds and creates one new Co_i–Co_i bond leading to the Co_{i-p} also as a p-type defect with -1 charge state (per Co) (see Figure 5). In addition, we found that the Co_{i-p} defect is difficult to form. In the Sb rich region, the p-type Co_v defect dominates. In addition to defect studies, the compositional range of binary CoSb₃ system is predicted.

2. METHODOLOGY

2.1. Crystal Structure of CoSb₃. The skutterudite CoSb₃ crystallizes in a cubic lattice (space group $Im\bar{3}$ (204), $a = 9.0385$ Å), in which the unit cell contains 8 Co and 24 Sb atoms occupying the 8c- and the 24g-sites, respectively (Figure 1a).²⁰ The Co atoms are octahedrally coordinated with Sb atoms (CoSb₆), and 4 Sb atoms are arranged into planar rectangular rings, each of which is oriented parallel to one of the unit cell edges. Co atoms form eight smaller cubes which contain 6 such Sb₄-rings (Figure 1b). In the unit cell two of the eight Co cubes remain empty.

2.2. Calculation Details. All density functional theory (DFT) calculations were performed with the Vienna ab initio Simulation Package (VASP) using the projector augmented wave (PAW) method with the Perdew–Burke–Ernzerhof (PBE) exchange-correlation functional.^{21–26} The 3s² 3p⁶ 3d⁸ 4s¹ electrons of Co and 5s² 5p³ electrons of Sb were treated as valence states to generate the PAW potentials. Here, “valence state” refers to the valence electron distribution, which is used to describe free electrons of elemental Co and Sb. The unit cell convergence test showed that a plane wave cutoff energy of 500 eV using a k -point grid set of $7 \times 7 \times 7$ Monkhorst–Pack scheme gives good convergence for the total energies. Our optimized lattice parameter is found to be $a = 9.115$ Å that is only 0.85% larger than the experimental value of 9.0385 Å²⁰ and consistent with the previous theoretical value of 9.14 Å using PBE.^{27–29} The calculated direct band gap of CoSb₃ is 0.186 eV as shown in Figure S1 in the Supporting Information, which agrees well with the 0.17 eV gap reported earlier.³⁰ All charged defect calculations are performed on a $2 \times 2 \times 2$ supercell of the cubic cell which contains 256 atoms, and the gamma only k -point for the sampling is used for all the supercells. Our optimized defect supercell can still remain the cubic crystallography of CoSb₃ because the lattice parameter of each charged supercell has a tiny change (<0.05%) compared with the ideal supercell, and no crystallographic distortions were observed in each charged defect supercell.

2.3. Defect Thermodynamics. The formation energy of a defect D in charge state q is defined as³¹

$$\Delta H_{D,q} = E_{D,q} - E_0 - \sum_i n_i \mu_i + q(E_v + \Delta E_{pa} + E_F) + \Delta E_{ic} \quad (1)$$

where $E_{D,q}$ is the total energy derived from a supercell calculation containing the defect D , and E_0 is the total energy of the perfect host supercell. The integer n_i represents the number of atoms of type i (host atoms or impurity atoms) which have been added to ($n_i > 0$) or removed from ($n_i < 0$) the supercell to form the defect, and μ_i are the corresponding atomic chemical potentials. E_v is the eigenvalue of the valence band maximum (VBM), E_F is the electron chemical potential (Fermi level at $T = 0$) referenced to the VBM, and ΔE_{pa} and ΔE_{ic} represent the potential alignment correction and image charge correction item in a charged supercell, respectively.^{32,33}

The concentration of a defect D in charge state q is given by

$$c_{D,q} = N_{site} \exp\left(-\frac{\Delta H_{D,q} - T\Delta S}{kT}\right) \quad (2)$$

where N_{site} is the concentration of possible defect sites, which is determined by the multiplicity of the defect's Wyckoff site. ΔS is the configurational entropy change, which is estimated by¹⁹

$$\Delta S = k\{\ln[N_D(N_D - 1)] - \ln(2N_D)\} \quad (3)$$

where N_D is the number of available sites in a fixed concentration of a specific defect D .

All the defect thermodynamics calculation is time-independent. The charge neutrality condition requires

$$\sum_D \sum_q q c_{D,q} - n + p = 0 \quad (4)$$

where n and p are the free carrier concentrations of electrons and holes given by³⁴

$$n = \int_{E_v}^{+\infty} g(E)f(E; E_F, T)dE \quad (5)$$

$$p = \int_{-\infty}^{E_c} g(E)[1 - f(E; E_F, T)]dE \quad (6)$$

$g(E)$ is the density of states of ideal host cell, and $f(E; E_F, T)$ is the Fermi–Dirac distribution given by

$$f(E; E_F, T) = \frac{1}{\exp\left(\frac{E - E_F}{kT}\right) + 1} \quad (7)$$

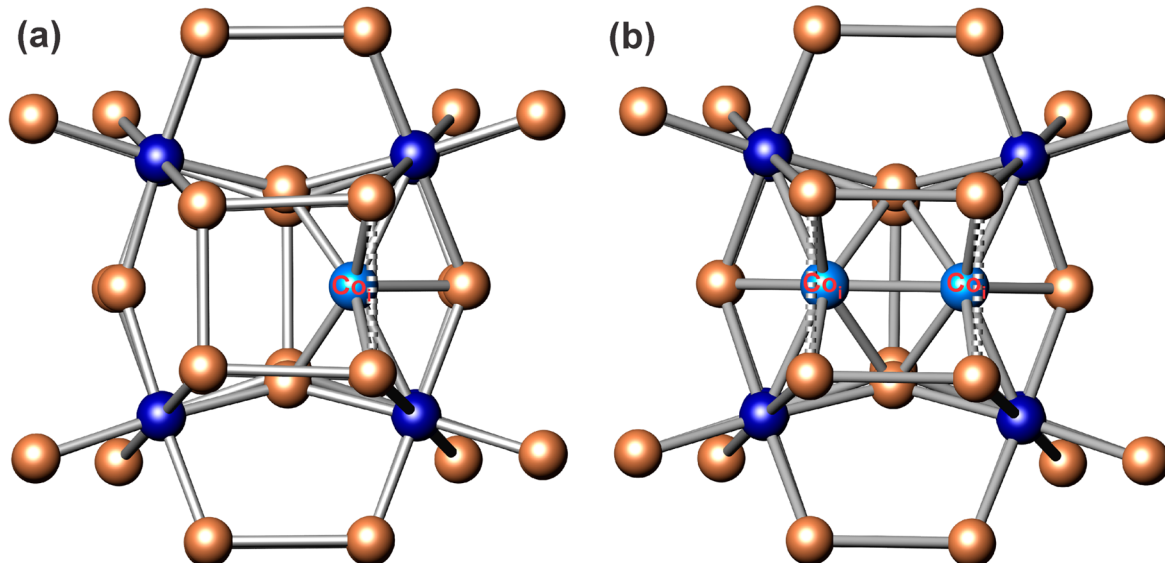


Figure 2. Crystal structure of CoSb_3 with (a) a single Co_i atom with 7-fold coordination and (b) a Co_{i-p} pair defect in the regular unit cell.

3. RESULTS AND DISCUSSION

3.1. Defect Formation Energy of Intrinsic CoSb_3 . We investigated the atomic structures of interstitial Co and Sb (Co_i and Sb_i) in CoSb_3 because there are several possible interstitial sites in CoSb_3 .¹⁹ The Co_i with 7-fold coordination (Figure 2(a)) and the Sb_i in the void center site are calculated to be the most stable single-defect structures. The total energy of the neutral Co_i structure in the cubic unit cell is 0.34 eV less than the Co_i with 6-fold coordination¹⁹ and 2.39 eV less than the Co_i in the void center site. The total energy of the structure with Sb_i in the void center site is 1.79 and 0.79 eV less than Sb_i with coordination numbers 6 and 7, respectively. In addition, the total energy of the neutral Co_{i-p} structure in the cubic unit cell (Figure 2(b)) is found to be 0.23 eV less than that with neutral Co_i , which agrees with Park's unit cell results.¹⁹

Seven typical point defects are considered in CoSb_3 : interstitials (Co_i , Sb_i), interstitial pairs (Co_{i-p}), antisites (Co_{Sb} , Sb_{Co}), and vacancies (Co_v , Sb_v). Various charged states were calculated for all defects. Here, "charge state" is used to describe the net charge of defects in the crystal structure. The defect formation energy as a function of E_F both in Co rich and Sb rich regions is shown in Figure 3. The slope of the curve reflects the charge state of each defect. For CoSb_3 , the Co rich region corresponds to the presence of CoSb_2 and CoSb_3 , whereas the Sb rich region corresponds to the presence of CoSb_3 and Sb.

In the Co rich region, the defect Co_{i-p} with -1 charge state per Co has the lowest formation energy in the band gap, implying that Co_{i-p} should be the dominant p-type defect. The formation energy of neutral Co_i and Co_{i-p} is 1.296 and 1.126 eV, respectively. Such high formation energy leads to a low number of carriers in the system (Figure 7(b)). The decomposing reaction of $\text{Co}_{i-p}^0 \rightarrow 2\text{Co}_i^0$ is considered between the neutral Co_{i-p} and Co_i defects. The Co_{i-p} will eventually lead to Co_i at high temperatures. For example, when the carrier concentration reaches to $5 \times 10^{18} \text{ cm}^{-3}$, the decomposition temperature of Co_{i-p} is found to be 390 K (Figure S2 in the Supporting Information), which is very low compared with the synthesis temperature (about 800–1100 K) of CoSb_3 ,^{10–15} indicating Co_{i-p} is difficult to form. Therefore, the isolated Co_i defect is the dominant defect in the Co rich region. That means each Co_i defect removes one electron from the CoSb_3 system,

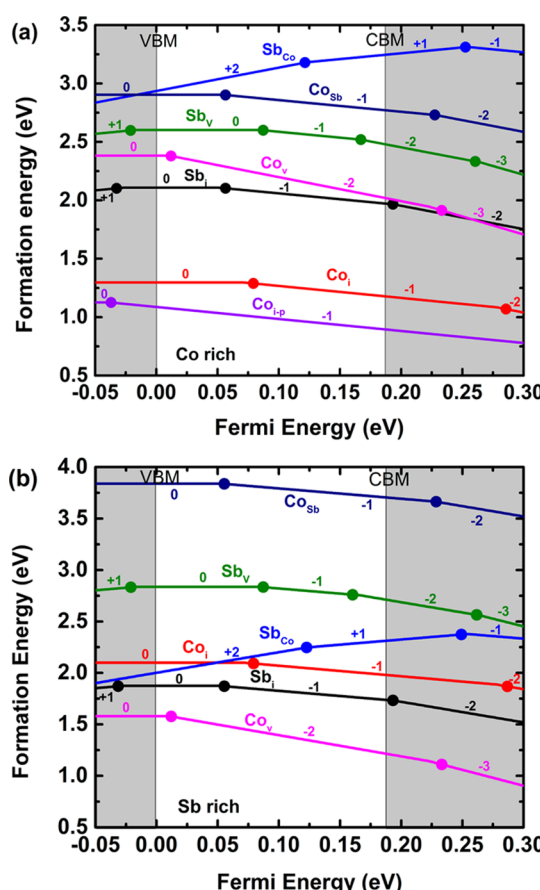


Figure 3. Calculated defect formation energy as a function of E_F (a) in Co rich and (b) in Sb rich regions. The white area represents the band gap region.

leading more holes than free electrons in the p-type CoSb_3 . In the Sb rich region, the Co_v defect has the lowest formation energy indicating that Co_v is the dominant defect which also removes electrons and introduces a p-type character.

3.2. Atomic Explanation of p-Type Intrinsic Defect in CoSb_3 . The presence of the Co_i interstitial dramatically

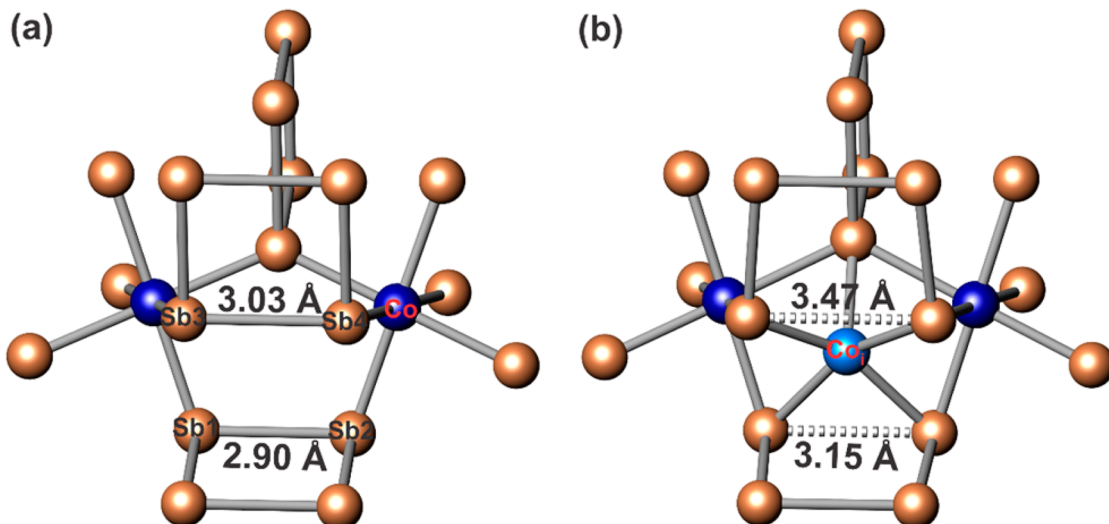


Figure 4. Coordination of the Co and Sb atoms: (a) in the ideal supercell and (b) in the supercell of neutral Co_i defect.

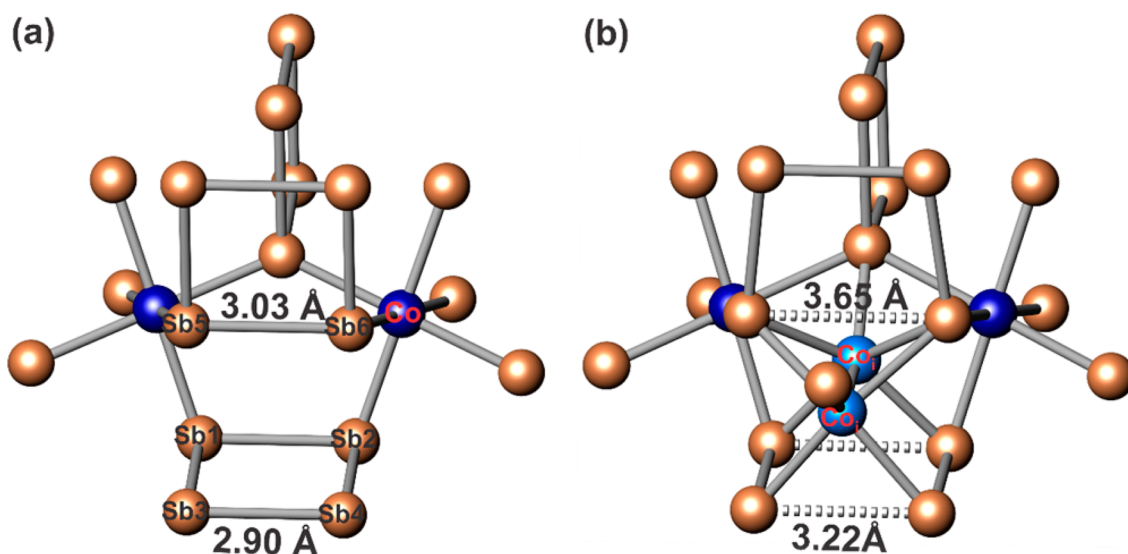


Figure 5. Coordination of the Co and Sb atoms (a) in the ideal supercell and (b) in the supercell of neutral Co_{i-p} defect.

disrupts the structure, chemically breaking two Sb–Sb bonds in two Sb_4 -rings, as shown in Figure 4. Specifically, Sb1–Sb2 interatomic distances change from 2.90 to 3.15 Å after inserting the Co_i defect, and Sb3–Sb4 interatomic distances change from 3.03 to 3.47 Å. A typical Sb–Sb bonding distance is considered to be ~ 2.9 Å as observed in Zn_4Sb_3 ³⁵ and CaSb_2 ³⁶ and distances greater than ~ 3.1 Å may point to weaker or nonbonding interactions.³⁷ Our results predict that the presence of Co_i increases the Sb–Sb bond length to 3.15 and 3.47 Å, respectively, indicating the breakage of these two Sb–Sb bonds, which agrees with the available structural data.^{35–37} The breakage of these two Sb–Sb σ -type bonds moves down Sb–Sb antibonding states to produce 4 new lone pairs that require 4 additional electrons as demonstrated in some intermetallic clathrates (e.g., BaGe_5 and $\text{Ba}_8\text{Ge}_{43}$) containing vacancies in the crystal structures.^{38–40} The Co_i atom itself is expected to behave chemically like the other Co atoms with valence Co^{3+} providing three electrons to the Co–Sb interacting system. Thus, the Co_i induced breakage of two Sb–Sb bonds must accept one more electron from the system, making Co_i an acceptor impurity with -1 charge state.

Similarly, the presence of the Co interstitial pair (Co_{i-p}) chemically breaks three Sb–Sb bonds in two Sb_4 -rings, as shown in Figure 5. Specifically, Sb1–Sb2 and Sb3–Sb4 interatomic distances change from 2.90 to 3.22 Å, and Sb5–Sb6 distances change from 3.03 to 3.65 Å after inserting the Co_{i-p} defect. The breakage of these three σ -type Sb–Sb bonds leaves six lone pairs of electrons. The Co_{i-p} could provide six additional electrons needed to satisfy the Sb states. However, the Co_{i-p} pair makes an additional Co–Co bond (2.38 Å) similar to Co–Co pairs as observed in other compounds, e.g., $\text{SmCo}_{9.8}$, $\text{Fe}_{1-x}\text{Co}_x\text{Ga}_3$, and $\text{Ho}_{12}\text{Co}_5\text{Bi}$.^{41–43} Co 3d states are split into three t_{2g} -like nonbonding states with energy lower than the two e_g -like states. Co_i – Co_i bond splits the e_g -like states turning one into a bonding state that requires two more electrons. So, ultimately, the Co_{i-p} behaves as an acceptor impurity with -1 charge state per Co_i , which also agrees well with our defect formation energy calculation.

The presence of Co_v does not change the local structure significantly, as shown in Figure 6. Six Sb atoms around a Co atom in CoSb_3 form an octahedron with Co–Sb bond length of 2.52 Å. When the Co atom is removed from the system, the Sb

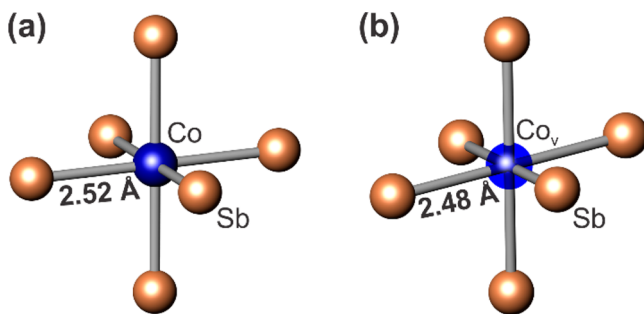


Figure 6. Coordination of the Co and Sb atoms: (a) in the ideal supercell and (b) in the supercell of neutral Co_v defect (shown with transparent blue sphere).

atoms move 0.04 Å closer to Co_v while preserving the octahedron environment. In CoSb_3 , the Co^{3+} atoms donate three electrons to the Co–Sb electronic structure suggesting that a Co_v should make the Co–Sb structure deficient by three electrons and therefore act as a p-type (e^- acceptor) impurity with -3 charge state.

Our calculations, however, suggest that the defect Co_v^{2-} is more stable than Co_v^{3-} for E_F within the band gap, as shown in Figure 3(b), which could be due to uncertainty in the localization of the charge or the calculations.⁴⁴ The ab initio point charge defect calculation assumes the dilute limit and negligible defect–defect interactions. When performing the supercell approach, the defect–defect interactions may affect the calculated formation energies, especially for the semiconductors with narrow band gap.⁴⁴ In the case of semiconductor CoSb_3 with a narrow band gap of 0.186 eV, we chose a cubic supercell with 256 atoms, being the calculation limit of CoSb_3 in ab initio VASP method. When performing Co_v^{3-} charge defect calculation, the concentration of negative excess charge ($4 \times 10^{21} \text{ cm}^{-3}$) is so high that it is very hard to completely remove the nonlocalized effect of the charged supercell, even though we added the potential alignment correction and image charge correction in the formation energy calculation. Even if only the chemically expected defects Co_i^{1-} and Co_v^{3-} were to dominate the defect thermodynamics of CoSb_3 , there would be little qualitative difference in the expected carrier concentration, as shown in Figure 7(b).

Our formation energy calculation results using PBE is different from that using LDA. It is generally known that the defect conductivity behavior depends on which charged defect has the lowest formation energy in the band gap region. For CoSb_3 , PBE predicted that $\text{Co}_{i,p}^{1-}$ is a p-type impurity because $\text{Co}_{i,p}^{1-}$ has the lowest formation energy in the band gap, but LDA predicted that it is an n-type impurity because $\text{Co}_{i,p}^{1+}$ has the lowest formation energy.¹⁹ Thus, the different defect conductivity behavior between PBE and LDA arises from different defect formation energy prediction of CoSb_3 . The PBE functional has been shown to be reliable for calculating various properties of CoSb_3 such as defect formation energy, cohesive energy, electronic states, effective mass, band gap, and bulk modulus.^{45–52} For example, the predicted defect formation energy and cohesive energy using PBE agrees well with the experiments.^{45–49} Ishii et al. found that the PBE valence bands can reproduce well the experimental ultraviolet photoemission spectroscopy data of CoSb_3 .⁵² The calculated effective mass and band gap of CoSb_3 using PBE are in excellent agreement with the experiments.^{18,51} However, LDA significantly overestimates the band gap, bulk modulus, and binding energy of CoSb_3 .⁴⁵

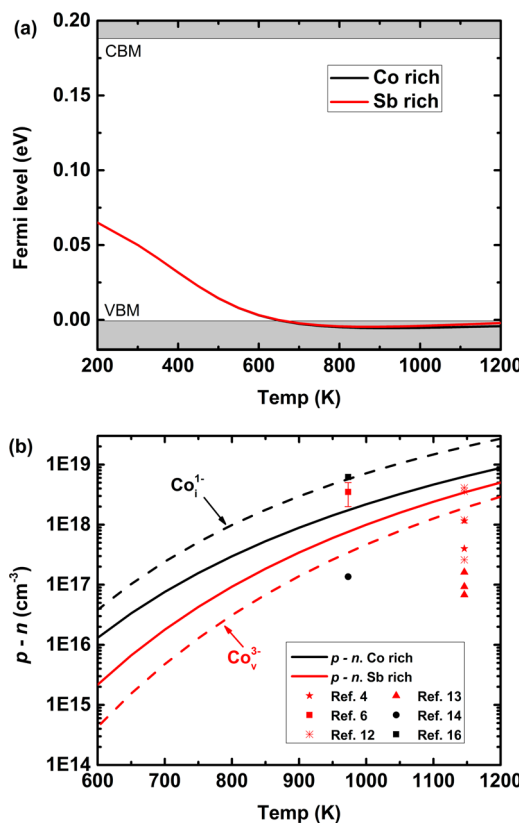


Figure 7. Calculated (a) E_F and (b) free carriers as a function of temperature. Experimental values of 300 K Hall carrier concentration vs annealing temperature for p-type samples are shown for comparison. The black lines and points represent the Co-rich environment, while red is used for Sb-rich. Black solid and dashed lines represent the thermodynamics calculation based on all defects and Co_i^{1-} defect only, respectively. Red solid and dashed lines represent the thermodynamics calculation based on all defects and Co_v^{3-} defect only, respectively.

Thus, we believe that the PBE functional can correctly predict the defect formation energy of CoSb_3 .

There are some relevant spin orbit contributions to the electronic structure in CoSb_3 , but the spin orbit interaction has little effect on the elastic properties of CoSb_3 such as the lattice parameter and bulk modulus.^{50,53} Meanwhile, the calculated effective mass and band gap using PBE functional are in excellent agreement with the experiments.^{18,51} More importantly, we have already tested the influence of spin orbit interactions on defect formation energy of CoSb_3 . The calculated formation energy of neutral Co_i defect with spin orbit interactions is only 0.04 eV lower than that without spin orbit interactions. Thus, spin orbit interactions have little effect on the defect formation energy of CoSb_3 .

3.3. Equilibrium Carriers and Phase Diagram of Intrinsic CoSb_3 . The calculated defect formation energy can predict the dominant defect type and conductivity behavior. The calculated phase diagram can predict the solubility ranges of these dopants, which is helpful to prepare the pure phase nonstoichiometry material and optimize the carriers to improve the thermoelectric properties in the field of thermoelectric research.

Following the procedure delineated in eqs 2–7, E_F and the number of free carriers of CoSb_3 can be obtained as a function of temperature by iteratively solving the charge neutrality

condition, the results of which are plotted in Figure 7. Due to the light band and small density of states as shown in Figure S1, E_F rapidly decreases to the VBM and even crosses it with increasing temperature both in Co rich and Sb rich environments, resulting in p-type behavior. The hole carrier concentration in the Co rich region is higher than that in the Sb rich region because of the lower formation energy of Co_i in the Co rich region compared with that of Co_v in the Sb rich region. The temperature region of interest is likely to be the synthesis and annealing temperature of CoSb_3 which is generally between 800 K and 1150 K.^{4–16} Here the intrinsic free carriers are found to be 10^{17} – 10^{19} cm^{–3} as shown in Figure 7(b), which is the same range found experimentally for pure, p-type CoSb_3 .^{4–16}

With an equilibrium set of chemical potentials, the composition x of element i in CoSb_3 is given by

$$x = \frac{N_0^i + \Delta N^i}{\sum_i (N_0^i + \Delta N^i)} \quad (8)$$

where N_0^i is the nominal stoichiometry of element i ($i = \text{Co, Sb}$) in CoSb_3 , and ΔN^i is the change in the composition due to the point defect at specific temperature T . The change in composition of CoSb_3 is calculated by summing over the carriers of each defect j , weighted by the change in composition due to the defect

$$\Delta N^i = \sum_j N_j^i c_j \quad (9)$$

Following the above procedure, we obtained the binary phase diagram of CoSb_3 as a function of temperature. The calculated solvus boundaries between CoSb_3 and Sb as red line (the Sb rich region) and between CoSb_3 and CoSb_2 as black line (the Co rich region) are shown in Figure 8. Because of the lower

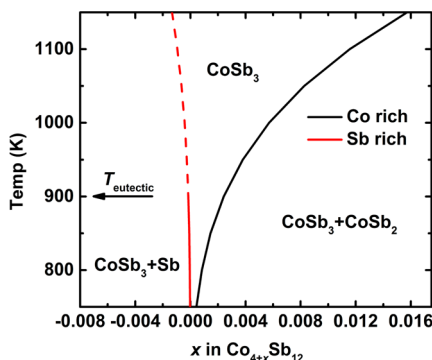


Figure 8. Predicted binary phase diagram of CoSb_3 as a function of temperature.

formation energy and higher concentration of Co_i in the Co rich region compared with that of Co_v in the Sb rich region, the solubility limit of CoSb_2 –Sb₃ boundary is much larger than that of the CoSb_3 –Sb boundary. The solvus boundaries indicate the solid equilibrium between CoSb_2 – CoSb_3 or CoSb_3 –Sb. The eutectic temperature of CoSb_3 –Sb is found to be 900 K suggesting that CoSb_3 is in equilibrium with liquid Sb, which indicates the solvus boundary of CoSb_3 –Sb is metastable above 900 K. For the CoSb_2 – CoSb_3 boundary, the peritectic temperature is 1150 K, indicating the solvus boundary of CoSb_2 – CoSb_3 is metastable above 1150 K.

4. CONCLUSIONS

We used density functional theory to study the native point defects of CoSb_3 to predict charge carrier concentration and nonstoichiometry. We found CoSb_3 is p-type in both Co rich and Sb rich regions. In the Co rich region, interstitial Co (Co_i) and Co interstitial pairs ($\text{Co}_{i,p}$) have the lowest formation energy and should be the dominant defects. However, due to the low decomposition temperature of $\text{Co}_{i,p}$, the Co interstitial pairs are not expected to form during the synthesis process of CoSb_3 . The breakage of Sb₄ rings induced by Co_i or $\text{Co}_{i,p}$ is found to be the main source of the unexpected acceptor nature due to the formation of lone pairs of electrons on Sb. In the Sb rich region, Co_v is the dominant p-type defect. Furthermore, we calculated the phase diagram of the binary CoSb_3 system and predict that the solubility limit of CoSb_3 in the Co rich region is larger than that in the Sb rich region.

■ ASSOCIATED CONTENT

Supporting Information

The Supporting Information is available free of charge on the ACS Publications website at DOI: [10.1021/acs.chemmater.6b00112](https://doi.org/10.1021/acs.chemmater.6b00112).

Electronic states of CoSb_3 and relative portion of Co_i and $\text{Co}_{i,p}$ as a function of the temperature (PDF)

■ AUTHOR INFORMATION

Corresponding Authors

*E-mail: jeff.snyder@northwestern.edu.

*E-mail: wag@wag.caltech.edu.

*E-mail: zhangqj@whut.edu.cn.

Notes

The authors declare no competing financial interest.

■ ACKNOWLEDGMENTS

This work is partially supported by National Basic Research Program of China (973-program) under Project No. 2013CB632505, the 111 Project of China under Project No. B07040, Materials Project by Department of Energy Basic Energy Sciences Program under Grant No. EDCBEE, DOE Contract DE-AC02-05CH11231, and China Postdoctoral Science Foundation (408-32200031). U.A. acknowledges the financial assistance of The Scientific and Technological Research Council of Turkey. H.X. and W.A.G. were supported by the National Science Foundation (DMR-1436985, program manager, John Schlueter).

■ REFERENCES

- (1) Snyder, G. J.; Toberer, E. S. Complex Thermoelectric Materials. *Nat. Mater.* **2008**, *7*, 105–114.
- (2) Rull-Bravo, M.; Moure, A.; Fernandez, J. F.; Martin-Gonzalez, M. Skutterudites as Thermoelectric Materials: Revisited. *RSC Adv.* **2015**, *5*, 41653–41667.
- (3) Uher, C. In *Handbook of Thermoelectrics: Macro to Nano*; Rowe, D. M., Eds.; CRC Press: Boca Raton, FL, 2006; Chapter 34, pp 1–17.
- (4) Caillat, T.; Borshchevsky, A.; Fleurial, J. P. Properties of single crystalline semiconducting CoSb_3 . *J. Appl. Phys.* **1996**, *80*, 4442–4449.
- (5) Caillat, T.; Fleurial, J. P.; Borshchevsky, A. Bridgman-solution crystal growth and characterization of the skutterudite compounds CoSb_3 and RhSb_3 . *J. Cryst. Growth* **1996**, *166*, 722–726.
- (6) Sharp, J. W.; Jones, E. C.; Williams, R. K.; Martin, P. M.; Sales, B. C. Thermoelectric Properties of CoSb_3 and Related Alloys. *J. Appl. Phys.* **1995**, *78*, 1013–1018.

- (7) Kawaharada, Y.; Kuroaski, K.; Uno, M.; Yamanaka, S. Thermoelectric properties of CoSb_3 . *J. Alloys Compd.* **2001**, *315*, 193–197.
- (8) Kuznetsov, V. L.; Kuznetsova, L. A.; Rowe, D. M. Effect of partial void filling on the transport properties of $\text{Nd}_x\text{Co}_4\text{Sb}_{12}$ skutterudites. *J. Phys.: Condens. Matter* **2003**, *15*, 5035–5048.
- (9) Wojciechowski, K. T.; Tobola, J.; Leszczynski, J. Thermoelectric properties and electronic structure of CoSb_3 doped with Se and Te. *J. Alloys Compd.* **2003**, *361*, 19–27.
- (10) Liu, W. S.; Zhang, B. P.; Li, J. F.; Zhao, L. D. Thermoelectric property of fine-grained CoSb_3 skutterudite compound fabricated by mechanical alloying and spark plasma sintering. *J. Phys. D: Appl. Phys.* **2007**, *40*, 566–572.
- (11) Liu, W. S.; Zhang, B. P.; Li, J. F.; Zhao, L. D. Effects of Sb compensation on microstructure, thermoelectric properties and point defect of CoSb_3 compound. *J. Phys. D: Appl. Phys.* **2007**, *40*, 6784–6790.
- (12) Morelli, D. T.; Caillat, T.; Fleurial, J. P.; Borshchevsky, A.; Vandersande, J.; Chen, B.; Uher, C. Low-Temperature Transport Properties of P-Type CoSb_3 . *Phys. Rev. B: Condens. Matter Mater. Phys.* **1995**, *51*, 9622–9628.
- (13) Arushanov, E.; Fess, K.; Kaefer, W.; Kloc, C.; Bucher, E. Transport properties of lightly doped CoSb_3 single crystals. *Phys. Rev. B: Condens. Matter Mater. Phys.* **1997**, *56*, 1911–1917.
- (14) Zhou, Z. H.; Uher, C.; Jewell, A.; Caillat, T. Influence of point-defect scattering on the lattice thermal conductivity of solid solution $\text{Co}(\text{Sb}_{1-x}\text{As}_x)$ (3). *Phys. Rev. B: Condens. Matter Mater. Phys.* **2005**, *71*, 235209–1–235209–6.
- (15) Wen, P. F.; Li, P.; Zhang, Q. J.; Yi, F. J.; Liu, L. S.; Zhai, P. C. Effect of Cyclic Thermal Loading on the Microstructure and Thermoelectric Properties of CoSb_3 . *J. Electron. Mater.* **2009**, *38*, 1200–1205.
- (16) Mi, J. L.; Zhu, T. J.; Zhao, X. B.; Ma, J. Nanostructuring and thermoelectric properties of bulk skutterudite compound CoSb_3 . *J. Appl. Phys.* **2007**, *101*, 054314–1–054314–6.
- (17) Gibbs, Z. M.; Kim, H.-S.; Wang, H.; Snyder, G. J. Band Gap Estimation from Temperature Dependent Seebeck Measurement-Deviations from the $2eS$ maxTmax Relation. *Appl. Phys. Lett.* **2015**, *106*, 022112–1–022112–5.
- (18) Tang, Y. L.; Gibbs, Z. M.; Agapito, L. A.; Li, G. D.; Kim, H.-S.; Nardelli, M. B.; Curtarolo, S.; Snyder, G. J. Convergence of Multi-valley Bands as the Electronic Origin of High Thermoelectric Performance in CoSb_3 Skutterudites. *Nat. Mater.* **2015**, *14*, 1223–1228.
- (19) Park, C.-H.; Kim, Y.-S. Ab Initio Study of Native Point-Defects in CoSb_3 : Understanding off-Stoichiometric Doping Properties. *Phys. Rev. B: Condens. Matter Mater. Phys.* **2010**, *81*, 085206–1–085206–7.
- (20) Schmidt, T.; Klüche, G.; Lutz, H. D. Structure Refinement of Skutterudite-Type Cobalt Triantimonide, CoSb_3 . *Acta Crystallogr., Sect. C: Cryst. Struct. Commun.* **1987**, *43*, 1678–1679.
- (21) An, Q.; Goddard, W. A.; Cheng, T. Atomistic Explanation of Shear-Induced Amorphous Band Formation in Boron Carbide. *Phys. Rev. Lett.* **2014**, *113*, 095501–1–095501–5.
- (22) Ogata, S.; Li, J.; Yip, S. Ideal Pure Shear Strength of Aluminum and Copper. *Science* **2002**, *298*, 807–811.
- (23) Roundy, D.; Krenn, C. R.; Cohen, M. L.; Morris, J. W. Ideal Shear Strengths of fcc Aluminum and Copper. *Phys. Rev. Lett.* **1999**, *82*, 2713–2716.
- (24) Kresse, G.; Furthmüller, J. Efficiency of ab-initio Total Energy Calculations for Metals and Semiconductors Using a Plane-Wave Basis Set. *Comput. Mater. Sci.* **1996**, *6*, 15–50.
- (25) Kresse, G.; Furthmüller, J. Efficient Iterative Schemes for ab initio Total-Energy Calculations Using a Plane-Wave Basis Set. *Phys. Rev. B: Condens. Matter Mater. Phys.* **1996**, *54*, 11169–11186.
- (26) Kresse, G.; Joubert, D. From Ultrasoft Pseudopotentials to the Projector Augmented-Wave Method. *Phys. Rev. B: Condens. Matter Mater. Phys.* **1999**, *59*, 1758–1775.
- (27) Kim, H.; Kavirayani, M.; Thomas, J. C.; Van der Ven, A.; Uher, C.; Huang, B. L. Structural Order-Disorder Transitions and Phonon Conductivity of Partially Filled Skutterudites. *Phys. Rev. Lett.* **2010**, *105*, 265901–1–265901–4.
- (28) Guo, R. Q.; Wang, X. J.; Huang, B. L. Thermal Conductivity of Skutterudite CoSb_3 from First Principles: Substitution and Nanoengineering Effects. *Sci. Rep.* **2015**, *5*, 7806–1–7806–9.
- (29) Mahan, G. D. Good Thermoelectrics. *Solid State Phys.* **1998**, *51*, 81–157.
- (30) Sofo, J. O.; Mahan, G. D. Electronic structure of CoSb_3 : A narrow-band-gap semiconductor. *Phys. Rev. B: Condens. Matter Mater. Phys.* **1998**, *58*, 15620–15623.
- (31) Zhang, S. B.; Northrup, J. E. Chemical-Potential Dependence of Defect Formation Energies in GaAs - Application to Ga Self-Diffusion. *Phys. Rev. Lett.* **1991**, *67*, 2339–2342.
- (32) Lany, S.; Zunger, A. Accurate Prediction of Defect Properties in Density Functional Supercell Calculations. *Modell. Simul. Mater. Sci. Eng.* **2009**, *17*, 084002–1–084002–14.
- (33) Makov, G.; Payne, M. C. Periodic Boundary-Conditions in Ab-Initio Calculations. *Phys. Rev. B: Condens. Matter Mater. Phys.* **1995**, *51*, 4014–4022.
- (34) Bjerg, L.; Madsen, G. K. H.; Iversen, B. B. Ab initio Calculations of Intrinsic Point Defects in ZnSb . *Chem. Mater.* **2012**, *24*, 2111–2116.
- (35) Jette, E. R.; Foote, F. Precision Determination of Lattice Constants. *J. Chem. Phys.* **1935**, *3*, 605–616.
- (36) Snyder, G. J.; Christensen, M.; Nishibori, E.; Caillat, T.; Iversen, B. B. Disordered Zinc in Zn_4Sb_3 with Phonon-Glass and Electron-Crystal Thermoelectric Properties. *Nat. Mater.* **2004**, *3*, 458–463.
- (37) Papoian, G. A.; Hoffmann, R. Hypervalent Bonding in One, Two, and Three Dimensions: Extending the Zintl-Klemm Concept to Nonclassical Electron-Rich Networks. *Angew. Chem., Int. Ed.* **2000**, *39*, 2408–2448.
- (38) Aydemir, U.; Akselrud, L.; Carrillo-Cabrera, W.; Candolfi, C.; Oeschler, N.; Baitinger, M.; Steglich, F.; Grin, Y. BaGe_5 : A New Type of Intermetallic Clathrate. *J. Am. Chem. Soc.* **2010**, *132*, 10984–10985.
- (39) Aydemir, U.; Candolfi, C.; Borrman, H.; Baitinger, M.; Ormeci, A.; Carrillo-Cabrera, W.; Chubilleau, C.; Lenoir, B.; Dauscher, A.; Oeschler, N.; Steglich, F.; Grin, Y. Crystal Structure and Transport Properties of $\text{Ba}_8\text{Ge}_{43}$ square(3). *Dalton. Trans.* **2010**, *39*, 1078–1088.
- (40) Nguyen, L. T. K.; Aydemir, U.; Baitinger, M.; Bauer, E.; Borrman, H.; Burkhardt, U.; Custers, J.; Haghaghirad, A.; Hofler, R.; Luther, K. D.; Ritter, F.; Assmus, W.; Grin, Y.; Paschen, S. Atomic Ordering and Thermoelectric Properties of the n-Type Clathrate $\text{Ba}_8\text{Ni}_{3.5}\text{Ge}_{42.1}$ square(0.4). *Dalton. Trans.* **2010**, *39*, 1071–1077.
- (41) Zhang, Z. X.; Song, X. Y.; Xu, W. W.; Li, D. P.; Liu, X. M. Crystal Structure and Magnetic Performance of Nanocrystalline $\text{SmCo}_{9.8}$ Alloy. *J. Appl. Phys.* **2011**, *110*, 124318–1–124318–5.
- (42) Tkachuk, A. V.; Mar, A. Structure and Physical Properties of Ternary Rare-Earth Cobalt Bismuth Intermetallics $(\text{RE})_{12}\text{Co}_3\text{Bi}$ ($\text{RE} = \text{Y}, \text{Gd}, \text{Tb}, \text{Dy}, \text{Ho}, \text{Er}, \text{Tm}$). *Inorg. Chem.* **2005**, *44*, 2272–2281.
- (43) Verchenko, V. Y.; Likhanov, M. S.; Kirsanova, M. A.; Gippius, A. A.; Tkachev, A. V.; Gervits, N. E.; Galeeva, A. V.; Büttgen, N.; Krätschmer, W.; Lue, C. S.; Okhotnikov, K. S.; Shevelkov, A. V. Intermetallic Solid Solution $\text{Fe}_{1-x}\text{Co}_x\text{Ga}_3$: Synthesis, Structure, NQR Study and Electronic Band Structure Calculations. *J. Solid State Chem.* **2012**, *194*, 361–368.
- (44) Freysoldt, C.; Grabowski, B.; Hickel, T.; Neugebauer, J.; Kresse, G.; Janotti, A.; Van de Walle, C. G. First-Principles Calculations for Point Defects in Solids. *Rev. Mod. Phys.* **2014**, *86*, 253–305.
- (45) Hammerschmidt, L.; Schlecht, S.; Paulus, B. Electronic Structure and the Ground-State Properties of Cobalt Antimonide Skutterudites: Revisited with Different Theoretical Methods. *Phys. Status Solidi A* **2013**, *210*, 131–139.
- (46) Xi, L. L.; Yang, J.; Lu, C. F.; Mei, Z. G.; Zhang, W. Q.; Chen, L. D. Systematic Study of the Multiple-Element Filling in Caged Skutterudite CoSb_3 . *Chem. Mater.* **2010**, *22*, 2384–2394.
- (47) Shi, X.; Zhang, W.; Chen, L. D.; Yang, J. Filling Fraction Limit for Intrinsic Voids in Crystals: Doping in Skutterudites. *Phys. Rev. Lett.* **2005**, *95*, 185503–1–185503–4.
- (48) Shi, X.; Zhang, W.; Chen, L. D.; Yang, J.; Uher, C. Thermodynamic Analysis of the Filling Fraction Limits for Impurities

in CoSb_3 Based on Ab Initio Calculations. *Acta Mater.* **2008**, *56*, 1733–1740.

(49) Tang, Y. L.; Qiu, Y. T.; Xi, L. L.; Shi, X.; Zhang, W. Q.; Chen, L. D.; Tseng, S. M.; Chen, S. W.; Snyder, G. J. Phase Diagram of In–Co–Sb System and Thermoelectric Properties of In-Containing Skutterudites. *Energy Environ. Sci.* **2014**, *7*, 812–819.

(50) Koga, K.; Akai, K.; Oshiro, K.; Matsuura, M. Electronic Structure and Optical Properties of Binary Skutterudite Antimonides. *Phys. Rev. B: Condens. Matter Mater. Phys.* **2005**, *71*, 155119-1–155119-9.

(51) Sofo, J. O.; Mahan, G. D. Electronic Structure of CoSb_3 : A Narrow-band-gap Semiconductor. *Phys. Rev. B: Condens. Matter Mater. Phys.* **1998**, *58*, 15620–15623.

(52) Ishii, H.; Okazaki, K.; Fujimori, A.; Nagamoto, Y.; Koyanagi, T.; Sofo, J. O. Photoemission Study of the Skutterudite Compounds CoSb_3 and RhSb_3 . *J. Phys. Soc. Jpn.* **2002**, *71*, 2271–2275.

(53) Li, G. D.; An, Q.; Li, W. J.; Goddard, W. A.; Zhai, P. C.; Zhang, Q. J.; Snyder, G. J. Brittle Failure Mechanism in Thermoelectric Skutterudite CoSb_3 . *Chem. Mater.* **2015**, *27*, 6329–6336.